communications physics

ARTICLE

https://doi.org/10.1038/s42005-023-01168-2 OPEN

Optimized frequency comb spectrum of parametrically modulated bottle microresonators

Manuel Crespo-Ballesteros [1✉], Andrey B. Matsko [2] & Misha Sumetsky[1]

Optical frequency combs generated by parametric modulation of optical microresonators are usually described by lumped-parameter models, which do not account for the spatial distribution of the modulation. This study highlights the importance of this spatial distribution in the Surface Nanoscale Axial Photonics (SNAP) platform, specifically for elongated SNAP bottle microresonators with a shallow nanometre-scale effective radius variation along its axial length. SNAP bottle microresonators have much smaller free spectral range and may have no dispersion compared to microresonators with other shapes (e.g., spherical and toroidal), making them ideal for generating optical frequency combs with lower repetition rates. By modulating parabolic SNAP bottle microresonators resonantly and adiabatically, we show that the flatness and bandwidth of the optical frequency comb spectra can be enhanced by optimizing the spatial distribution of the parametric modulation. The optimal spatial distribution can be achieved experimentally using piezoelectric, radiation pressure, and electro-optical excitation of a SNAP bottle microresonator.

[1] Aston Institute of Photonic Technologies, Aston University, Birmingham B4 7ET, UK. [2] Jet Propulsion Laboratory, California Institute of Technology, Pasadena, CA 91109, USA. ✉email: m.crespo@aston.ac.uk

The generation of optical frequency combs (OFCs) represents a vibrant field of research in photonics[1,2] with numerous applications in precision spectroscopy, optical metrology, and high-speed optical communications[3–6]. Currently, the main techniques to generate OFCs use mode-locked lasers[7], electro-optic (EO) modulation of continuous wave lasers[8], and nonlinear optical processes in microresonators[9,10]. The most common method to generate OFCs in microresonators is based on the nonlinear Kerr effect[11–14], but alternative approaches have been proposed, such as the application of the EO effect in microresonators made of materials with second-order nonlinearity[15–20]. The microresonator-based comb technologies are particularly attractive because they offer compact, efficient, and high-repetition-rate frequency combs (of the order of GHz and THz). However, applications such as high-precision spectroscopy require OFCs with lower repetition rates (a few hundreds of MHz or smaller)[3,21], which is more challenging to achieve with microresonators. Indeed, the repetition rate frequency of microresonator-based OFCs is usually equal to the microresonator free spectral range (FSR), $\Delta\nu_{\mathrm{FSR}}$, which, for the commonly used ring, toroidal, and spherical microresonators, is inversely proportional to their size. As an example, a silica toroidal or spherical microresonator with $\Delta\nu_{\mathrm{FSR}} = 50$ MHz has a radius $r_0 = c/(2\pi n_0 \Delta\nu_{\mathrm{FSR}}) = 65$ cm (here c is the speed of light and $n_0 = 1.46$ is the refractive index of silica). Therefore, to achieve sufficiently low repetition rates, the microresonator size has to be increased to dimensions which may be unpractical.

One approach to solve the challenge of generating OFCs with low repetition rates in microresonators consists in the adiabatic modulation of microresonator parameters at frequency ν_{par} that is much smaller than its FSR, $\nu_{\mathrm{par}} \ll \Delta\nu_{\mathrm{FSR}}$. In this case, the repetition rate of the OFC is equal to the modulation frequency and independent of the microresonator size. In a recent paper[22], the authors demonstrated a flat frequency comb spectrum with repetition rate as low as 50 MHz generated by optomechanical oscillations of a toroidal silica microresonator. The adiabatically slow modulation of the microresonator eigenfrequency depends on time as $\nu_e(t) = \nu_{e0} + \delta\nu_{\mathrm{par}}\cos(2\pi\nu_{\mathrm{par}}t)$, where $\delta\nu_{\mathrm{par}}$ is the amplitude of modulation. This modulation can generate a close to uniform OFC formed by $N \cong \delta\nu_{\mathrm{par}}/\nu_{\mathrm{par}}$ spectral resonances separated by the modulation frequency ν_{par} (see consideration below). For a microresonator with radius r_0, the parametric modulation corresponds to an amplitude change of the effective radius variation (ERV) defined by the scaling relation $\delta r_{\mathrm{eff}} = r_0\delta\nu_{\mathrm{par}}/\nu_{e0}$. For the experimental parameters in the work of Hu et al.[22], $r_0 \cong 30$ μm, $\nu_{e0} \cong 200$ THz, $\nu_{\mathrm{par}} = 50$ MHz, and $N \cong 1000$, we find $\delta r_{\mathrm{eff}} \cong 8$ nm. In ref. [22], this modulation was generated by the radiation pressure of the resonant high-power input light that excited the mechanical breathing mode of the microresonator.

The application of SNAP bottle microresonators (SBMs) with shallow nanoscale ERV, which are introduced at the surface of optical fibres[23–27], constitutes an alternative and promising approach to generate OFCs with low repetition rates. Optical eigenmodes in SNAP microresonators are whispering gallery modes (WGMs) adjacent to the fibre surface and slowly bouncing between turning points along the microresonator axial length. The adiabatic generation of OFCs with low repetition rates can be realized in SBMs by a strong input light, similar to the approach of Hu et al.[22]. Alternatively, the EO modulation of the microresonator refractive index can also be used to generate OFCs (see[15,18,19] and references therein). The FSR of a SBM is estimated as $\Delta\nu_{\mathrm{FSR}} = c(2\pi n_0)^{-1}(r_0R)^{-1/2}$ where r_0 is the fibre radius, $R \gg r_0$ represents the axial radius, and n_0 is the refractive index of the microresonator material[23,24]. It is worth noting that for SBMs, the value of R can be dramatically large. For example, for the semi-parabolic SBM fabricated by Sumetsky[28], the axial radius was $R \cong 0.7$ km and, potentially, can be an order of magnitude greater. A feasible FSR for a silica ($n_0 = 1.46$) SBM with $R = 10$ km and $r_0 = 100$ μm is $\Delta\nu_{\mathrm{FSR}} \cong 33$ MHz. To maximise the frequency comb bandwidth, the SBM should have equally spaced axial eigenfrequencies. This feature is achievable with the SNAP technology as we can fabricate SBMs with parabolic or semi-parabolic shape[28]. Experimentally, OFCs generated by conventional bottle microresonators with axial radius R of the order of 100 μm have been presented by several groups[29–31] starting with the first demonstration by Savchenkov et al.[32]. The generation of OFCs in parabolic SBMs by the nonlinear Kerr effect and by resonant harmonic parametric excitation has been theoretically studied[33,34]. However, to the best our knowledge, OFCs generated by parametric modulation of parabolic SBMs have not been experimentally demonstrated to date.

In this paper, we theoretically investigate the formation of OFCs by the parametric modulation of parabolic SBMs going beyond the lumped-element model[15,18–20,22] and taking into account the spatial distribution of the parametric modulation (SDPM). Based on the theory of SNAP microresonators with time-dependent parameters[35], we optimize the SDPM targeting to arrive at the maximum flat and broadband OFC spectrum. Significantly, the characteristic ERV δr_{par} of the SDPM can be much smaller than, as well as comparable to, the dramatically small nanometre-scale ERV Δr_0 of the SBM. Below, we demonstrate the critical importance of the SDPM in the adiabatic ($\nu_{\mathrm{par}} \ll \Delta\nu_{\mathrm{FSR}}$) and resonant ($\nu_{\mathrm{par}} = 2\Delta\nu_{\mathrm{FSR}}$) cases as well as for relatively small ($\delta r_{\mathrm{par}} \ll \Delta r_0$) and large ($\delta r_{\mathrm{par}} \sim \Delta r_0$) modulation amplitudes.

Results and discussion

We consider a parabolic SBM formed by the nanoscale ERV of an optical fibre with radius r_0 illustrated in Fig. 1. Light is coupled into the SBM by a transverse optical waveguide placed at $z = z_0$. In our analysis, we model the input light as a monochromatic source $A_{\mathrm{in}}(z,t)\cdot e^{-2\pi i\nu_{\mathrm{par}}t}$ where function $A_{\mathrm{in}}(z,t)$ is localised near the point z_0 and has the characteristic switching time α^{-1}:

$$A_{\mathrm{in}}(z,t) = A_0\delta(z-z_0)\begin{cases}(1-e^{-\alpha t}) & t \geq 0\\ 0 & t<0\end{cases}. \qquad (1)$$

If frequency ν_{in} is close to one of the cutoff frequencies of the optical fibre $\nu_c(z,t)$[23], the input light excites a WGM that slowly propagates along z and bounces between the SBM turning points forming eigenmodes. The slowness of the propagating WGM depends on the proximity of its frequency ν_{in} to the cutoff frequency $\nu_c(z,t)$ which is assumed to have the parabolic shape perturbed by the parametric modulation:

$$\nu_c(z,t) = \nu_{c0} + \delta\nu_{\mathrm{par}}\cdot\xi(z/L)\cdot\sin\left(2\pi\nu_{\mathrm{par}}t\right) + \begin{cases}\Delta\nu_0\left[\left(\frac{z}{L}\right)^2-1\right] & |z|\leq L\\ 0 & |z|>L\end{cases}. \qquad (2)$$

Here, $2L$ is the length of the SBM, ν_{c0} is the cutoff frequency of the uniform optical fibre away from the SBM, $\Delta\nu_0$ is the maximum of the cutoff frequency variation (CFV) that forms the SBM (Fig. 1), $\delta\nu_{\mathrm{par}}$ is the maximum of the modulation amplitude, and $\xi(z/L)$ is its dimensionless spatial distribution.

For sufficiently small and slow deformation of the optical fibre, the WGM field distribution is separable in cylindrical coordinates as $e^{il\phi}\Theta_p(r)\Psi(z,t)\cdot e^{-i2\pi\nu_{\mathrm{in}}t}$, where l, and p, are the azimuthal and radial quantum numbers. Then, under the condition that $\nu_c(z,t)$

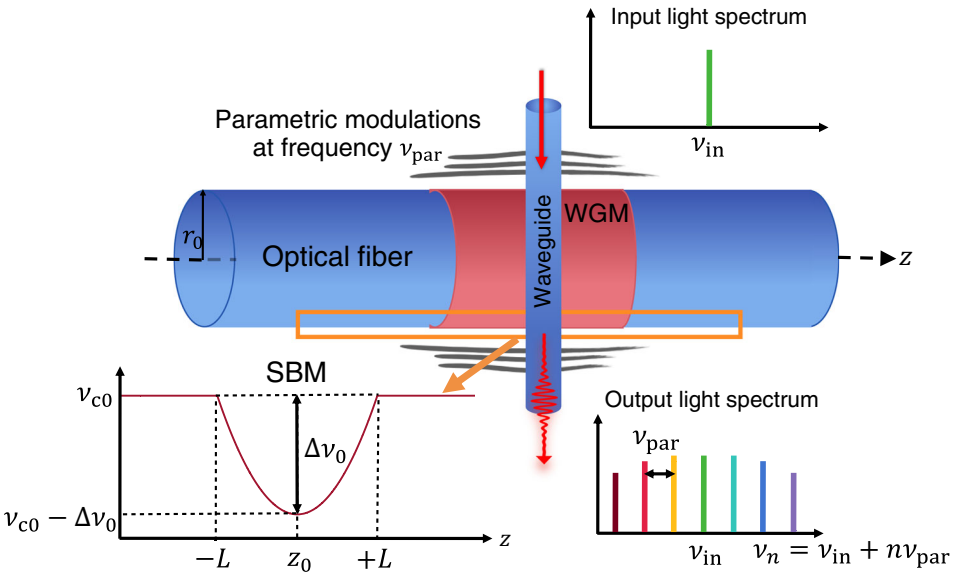

Fig. 1 Illustration of the considered system. A SNAP bottle microresonator (SBM) with parabolic cutoff frequency variation (CFV) centred at $z_0 = 0$ introduced at the surface of an optical fibre with radius r_0. The SBM is coupled to the transverse waveguide that pumps light at frequency ν_{in} and excites whispering gallery modes (WGMs). The SBM is parametrically modulated with frequency ν_{par} and generates an optical frequency comb at the output of the waveguide with the repetition rate ν_{par}.

is sufficiently close to ν_{in}, the function $\Psi(z,t)$ obeys the Schrödinger equation[35]:

$$\mathrm{i}\frac{1}{2\pi\nu_{c0}}\partial_t\Psi(z,t) = \Big[-\frac{1}{2\beta_{c0}^2}\partial_z^2 + \frac{\nu_c(z,t) - \nu_{in} - \mathrm{i}\gamma}{\nu_{c0}} - \frac{1}{\beta_{c0}^2}D_0\delta(z-z_0)\Big]\Psi(z,t) + A_{in}(z,t). \quad (3)$$

Here, $\beta_{c0} = 2\pi n_0\nu_{c0}/c$ is the cutoff wavenumber, n_0 is the refractive index of the SBM, and c is the speed of light. In Eq. (3), the absorption losses in the SBM are determined by the parameter γ while the complex number D_0 takes into account the effect of the input-output waveguide coupled to the SBM at $z = z_0$[23].

In the presence of coupling and losses, the frequencies of the SBM are complex-valued and given by

$$\widetilde{\nu}_q = \nu_q - \mathrm{i}\Gamma_q = \big(\nu_{c0} - \Delta\nu_0 + (q+1/2)\Delta\nu_{FSR} - \delta\nu_{D_0,q}\big) - \mathrm{i}\Gamma_q, \quad \Delta\nu_{FSR} = c/2\pi n_0 L\cdot\sqrt{2\Delta\nu_0/\nu_{c0}} \quad (4)$$

where q is the axial quantum number and $\Delta\nu_{FSR}$ is the axial FSR of the unmodulated SBM. Here $\delta\nu_{D_0,q}$ and Γ_q are the frequency shift and width induced by coupling and material losses[23],

$$\delta\nu_{D_0,q} = \frac{c^2}{8\pi^2 n_0^2\nu_{c0}}\mathrm{Re}(D_0)|\varphi_q(z_0)|^2, \quad \Gamma_q = \gamma + \frac{c^2}{8\pi^2 n_0^2\nu_{c0}}\mathrm{Im}(D_0)|\varphi_q(z_0)|^2. \quad (5)$$

In this equation, $\varphi_q(z)$ are the eigenmodes of Eq. (3) in the absence of source, parametric modulation, coupling effects, and losses ($A_0 = \delta\nu_{par} = D_0 = \gamma = 0$). From expression Eq. (5), the Q-factor of the eigenmode q is calculated as

$$Q_q = \frac{\nu_{in}}{\Gamma_q}. \quad (6)$$

The OFC spectrum is determined from the solution of Eq. (3) as follows. First, we calculate the Fourier transform of this solution at the position $z = z_0$ of the source, $F(\nu, z_0, \delta\nu_{par}) = \int \mathrm{d}t\exp(-2\pi\mathrm{i}\nu t)\Psi(z_0,t)$. Here, for convenience, the modulation amplitude $\delta\nu_{par}$ from Eq. (2) is included. Next, we normalise $F(\nu, z_0, \delta\nu_{par})$ by relating it to the maximum of the output spectrum at zero modulation amplitude, $\max\big[|F(\nu, z_0, 0)|\big]$. Then, the output OFC power spectrum is found as

$$P(\nu) = \left|\frac{F\big(\nu, z_0, \delta\nu_{par}\big)}{\max\big[|F(\nu, z_0, 0)|\big]}\right|^2 \quad (7)$$

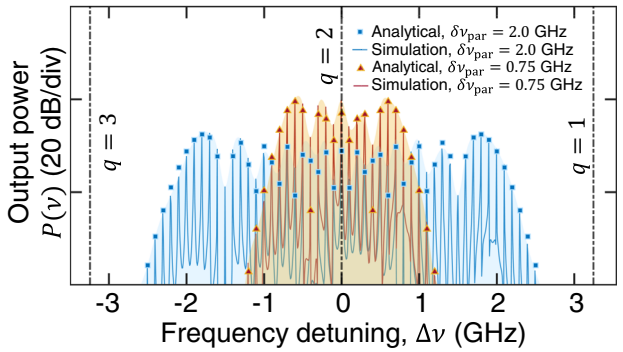

Fig. 2 Optical frequency combs (OFCs) generated by the spatially uniform adiabatic modulation of a parabolic SNAP bottle microresonator. The blue and red lines correspond to the OFC spectrum obtained from numerical solution of Eq. (3) for constant modulation amplitudes $\delta\nu_{par} = 2$ GHz (blue line) and $\delta\nu_{par} = 0.75$ GHz (orange line), respectively. In both cases, the Q-factor is $Q_{q_0} = 1.2\times10^7$. The blue squares and the orange triangles correspond to the spectrum found from Eq. (8) for $\delta\nu_{par} = 2$ GHz and $\delta\nu_{par} = 0.75$ GHz, respectively.

Below, we investigate the OFCs generated by the SBM determined by Eqs. (2) and (3) for the cases of adiabatically slow

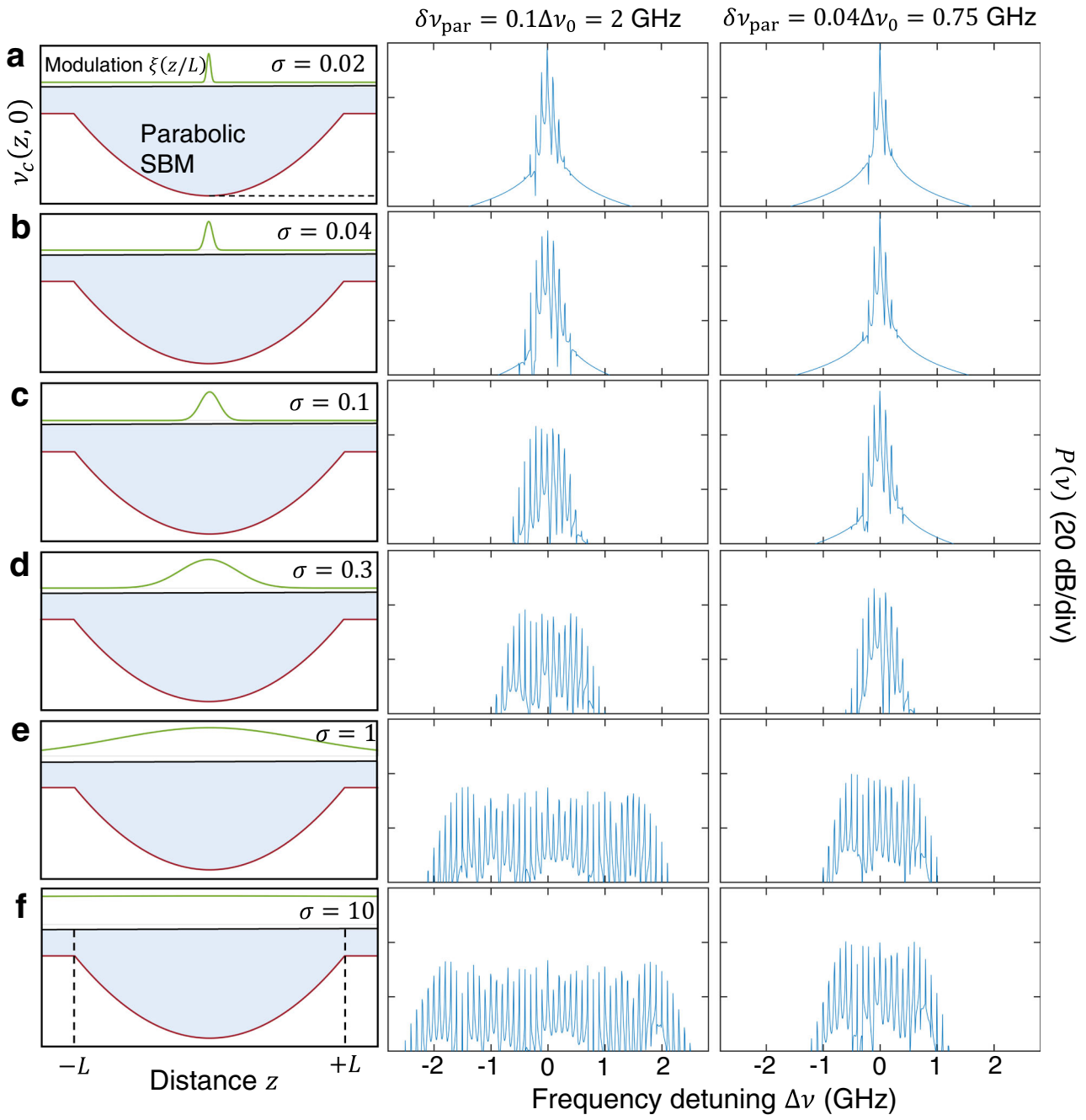

Fig. 3 Optical frequency combs (OFCs) generated by the adiabatic modulation of the parabolic SNAP bottle microresonator (SBM) with Gaussian spatial distribution of the modulations (SDPMs). The SDPM (green line) is defined by $\xi(z/L) = e^{-(z/\sigma\cdot L)^2}$, where σ is the dimensionless SDPM width and L is half the length of the SBM (red line). Rows show the OFC generated with different values of σ for two modulation amplitude maxima: $\delta\nu_{\mathrm{par}} = 0.1\Delta\nu_0 = 2$ GHz and $\delta\nu_{\mathrm{par}} = 0.04\Delta\nu_0 = 0.75$ GHz. **a** A limited number of comb resonances are formed at $\sigma = 0.02$ for both values of $\delta\nu_{\mathrm{par}}$, when the SDPM is strongly localized near the centre of the SBM. **b**–**e** The OFC spectrum becomes wider and flatter with growing σ. For $\delta\nu_{\mathrm{par}} = 0.75$ GHz, the OFC has a smaller bandwidth, though the power level is ~ 10 dB higher than in the case of $\delta\nu_{\mathrm{par}} = 2$ GHz. **f** The generated OFC achieves its optimal shape for a close to uniform SDPM, when $\sigma = 10$.

parametric modulation, $\nu_{\mathrm{par}} \ll \Delta\nu_{\mathrm{FSR}}$, and resonant parametric modulation, $\nu_{\mathrm{par}} = 2\Delta\nu_{\mathrm{FSR}}$.

Adiabatic parametric modulation of the SBM. In this section, we consider the adiabatic modulation of the SBM assuming that the frequency ν_{par} is much smaller than the microresonator FSR, $\nu_{\mathrm{par}} \ll \Delta\nu_{\mathrm{FSR}}$, and the OFC resonances are well defined so that their width is much smaller than their separation, i.e., $\Gamma_q \ll \nu_{\mathrm{par}}$. We set the input frequency ν_{in} equal to one of the SBM eigenfrequencies ν_{q_0}. The simplest parametric modulation corresponds to an axially uniform SDPM with $\xi(z/L) = 1$ and $\varepsilon(z,t) = \delta\nu_{\mathrm{par}} \cdot \sin(2\pi\nu_{\mathrm{par}}t)$. In this case, the transmission power spectrum $P(\nu)$

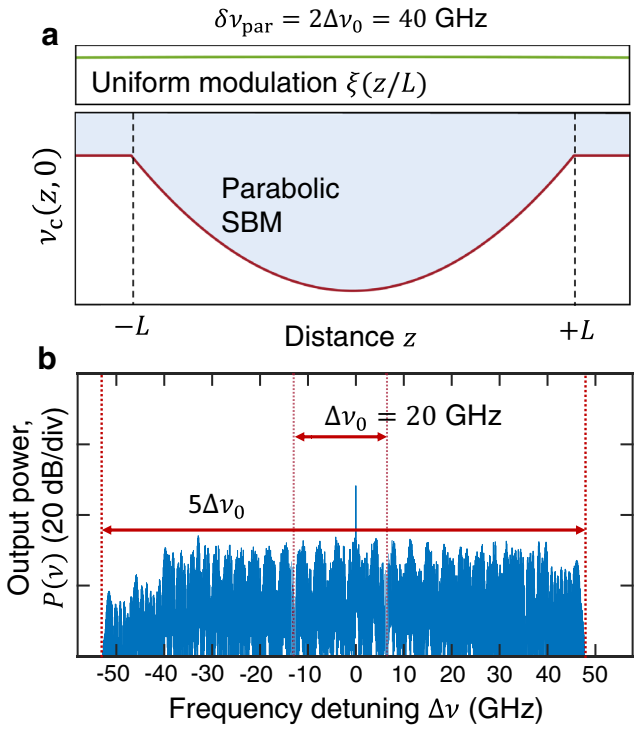

Fig. 4 Optical frequency comb (OFC) generated by a uniform adiabatic modulation with amplitude exciding the bandwidth of the SNAP bottle microresonator (SBM). a Adiabatic modulation of the parabolic SBM (red line) with a uniform spatial distribution $\xi(z/L)$ (green line). The maximum amplitude of the modulation is $\delta\nu_{\rm par} = 2\Delta\nu_0 = 40$ GHz. **b** The generated OFC has a bandwidth five times larger than that of the SBM, $\Delta\nu_0 = 20$ GHz. The number of comb lines generated are ~1000.

vanishes at frequencies $\nu \neq \nu_{q_0} + n\nu_{\rm par}$, $n = 0, \pm 1, \pm 2, \ldots$, and (see Methods)

$$P\left(\nu_{q_0} + n\nu_{\rm par}\right) = \left| J_n\left(\frac{\delta\nu_{\rm par}}{\nu_{\rm par}}\right) J_0\left(\frac{\delta\nu_{\rm par}}{\nu_{\rm par}}\right)\right|^2. \quad (8)$$

From this equation, the OFC spectrum is formed by a series of equally spaced resonances with magnitudes determined by the dependence of Bessel functions $J_n(\frac{\delta\nu_{\rm par}}{\nu_{\rm par}})$ on the comb resonance number n. From the asymptotic of the Bessel function for large order and argument, $|n|, \frac{\delta\nu_{\rm par}}{\nu_{\rm par}} \gg 1$, we find that the OFC spectrum determined by Eq. (8) is relatively flat within the bandwidth including $N \sim \frac{2\delta\nu_{\rm par}}{\nu_{\rm par}}$ resonances.

The comparison of the OFC spectrum obtained from the numerical solution of Eq. (3) with that given by Eq. (8) and shown in Fig. 2 demonstrates their excellent agreement. We consider an SBM with maximum CFV $\Delta\nu_0 = 20$ GHz, total length $2L = 284$ μm and radius $r_0 = 20$ μm. The input-output waveguide is placed at the centre of the SBM, $z_0 = 0$. The input light frequency is set to $\nu_{\rm in} = \nu_{c0} = 200$ THz which is equal to the SBM eigenfrequency ν_{q_0} with axial quantum number $q_0 = 2$. For these parameters, the axial FSR of the SBM determined by Eq. (4) is $\Delta\nu_{\rm FSR} = 3.25$ GHz. We analyse the OFCs generated with two different relatively small modulation amplitudes, $\delta\nu_{\rm par} = 0.1\Delta\nu_0 = 2$ GHz and $\delta\nu_{\rm par} = 0.04\Delta\nu_0 = 0.75$ GHz, at frequency $\nu_{\rm par} = 100$ MHz. From the scaling relation $\delta r_{\rm par} = r_0\delta\nu_{\rm par}/\nu_{c0}$, these amplitudes correspond to the ERV $\delta r_{\rm par} = 200$ pm and $\delta r_{\rm par} = 75$ pm, respectively, while the total ERV of the SBM considered is $\Delta r_0 = r_0\Delta\nu_0/\nu_{c0} = 2$ nm. The material attenuation and coupling coefficient are set to $\gamma = 2\pi$ MHz and $D_0 = 0.001(1 + {\rm i})$ $\mu{\rm m}^{-1}$, which corresponds to $Q_{q_0} = 1.2\times 10^7$ calculated from Eqs. (5) and (6).

We now investigate the effect of the SDPM, $\xi(z/L)$, on the generation of OFCs. We assume the Gaussian SDPM, $\xi(z/L) = {\rm e}^{-(z/\sigma L)^2}$, where the dimensionless parameter σ determines the ratio of characteristic SDPM width and SBM length $2L$. Excitation of a broader OFC spectrum at the minimum required power depends on the techniques to generate the parametric modulations. In particular, the required input power may be determined by the maximum amplitude of modulation, its integrated intensity, or by a more complex functional dependence of the modulation parameters on the input power. Here, we suggest that the required power is determined by the maximum amplitude of the SDPM and set the same $\delta\nu_{\rm par}$ for all the cases considered.

Figure 3 shows the results of our numerical simulations for the parabolic SBM (red line) with the parameters indicated above using Gaussian SDPMs (green line) with different values of σ. We present the OFC spectra of the signal obtained from Eq. (3) for two modulation amplitude maxima $\delta\nu_{\rm par} = 0.1\Delta\nu_0 = 2$ GHz and $\delta\nu_{\rm par} = 0.04\Delta\nu_0 = 0.75$ GHz, both much smaller that the maximum CFV of the SBM $\Delta\nu_0 = 20$ GHz. In the case $\sigma = 0.02$, the Gaussian SDPM is localized near the centre of the SBM as shown in Fig. 3a and the OFC spectrum exhibits only a few comb resonances. The spectrum of the frequency combs becomes wider and flater with growing σ (Fig. 3b–e). In the case $\sigma = 10$ shown in Fig. 3f, the parametric modulation has a close to the uniform SDPM over the whole length of the SBM and the spectrum coincides with that obtained from Eq. (8) and illustrated in Fig. 2.

So far, we considered the modulation of the SBM with maximum amplitudes $\delta\nu_{\rm par}$ much smaller than the full CFV $\Delta\nu_0 = 20$ GHz of the resonator. However, the dramatically small CFV and corresponding ERV of the SBM ($\Delta r_0 = 2$ nm in the cases considered) makes the modulations comparable or larger than the resonator CFV realistic as well. As an example, we modulate the same SBM with a uniform SDPM and maximum amplitude $\delta\nu_{\rm par} = 2\Delta\nu_0 = 40$ GHz (Fig. 4a). The corresponding ERV modulation amplitude is 4 nm (compare it with the 8 nm ERV oscillation amplitude experimentally achieved by Hu et al.[22] and discussed in the introduction). It is seen from Fig. 4b that, as expected, the generated OFC spectrum expands over the bandwidth $5\Delta\nu_0$ (from $\nu_{q_0} - 2.5\Delta\nu_0$ to $\nu_{q_0} + 2.5\Delta\nu_0$). The number of OFC resonances within the central most uniform part of this spectrum, from −40 to 40 GHz, is well estimated by $N \sim 2\delta\nu_{\rm par}/\nu_{\rm par} = 4\Delta\nu_0/\nu_{\rm par} = 800$, followed from the asymptotic of Eq. (8) discussed above, while the full bandwidth includes close to $5\Delta\nu_0/\nu_{\rm par} = 1000$ OFC resonances.

Resonant parametric modulation of the SBM. As in the previous section, we place the input light source in the middle of the SBM ($z_0 = 0$) so that the excited eigenmodes have even parity. Then, due to the symmetry of the system, transitions between eigenmodes of different parity are suppressed and the parametric modulation frequency has to be $\nu_{\rm par} = 2\Delta\nu_{\rm FSR}$ to achieve an effective resonant excitation of the SBM eigenmodes. In this case, the SBM has the maximum CFV $\Delta\nu_0 = 5$ GHz, the total length $2L = 9.18$ mm, and radius $r_0 = 80$ μm. The axial FSR of this SBM is $\Delta\nu_{\rm FSR} = 50$ MHz, so the resonant condition takes place at $\nu_{\rm par} = 2\Delta\nu_{\rm FSR} = 100$ MHz. The input light frequency is set

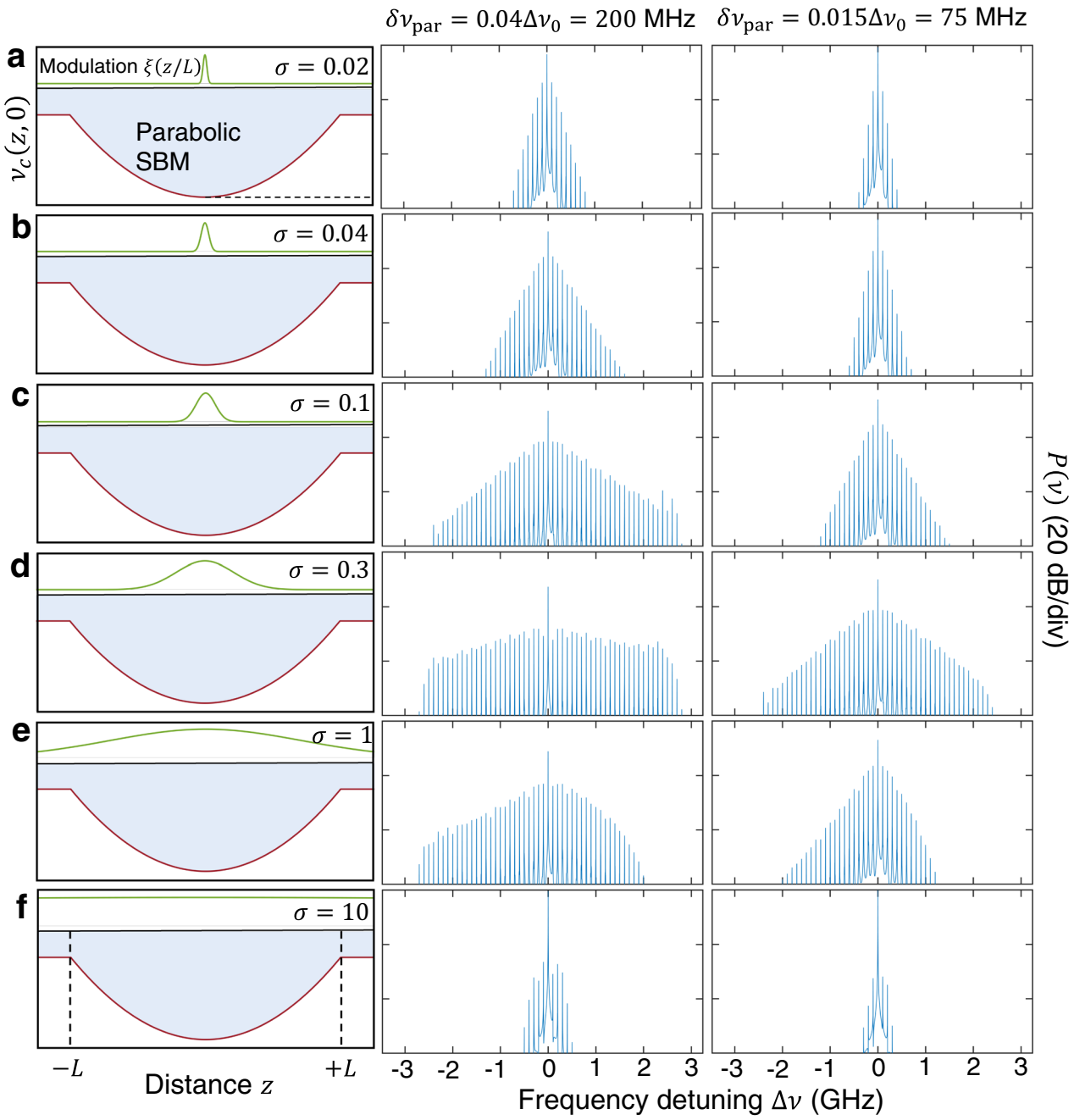

Fig. 5 Optical frequency combs (OFCs) generated with a Gaussian spatial distribution of the modulations (SDPMs) in the resonant regime. The parabolic SNAP bottle microresonator (SBM) (red line) is modulated with a Gaussian SDPM $\xi(z/L) = e^{-(z/\sigma L)^2}$ (green line) for two maximum modulation amplitudes, $\delta\nu_{\mathrm{par}} = 200$ MHz and $\delta\nu_{\mathrm{par}} = 75$ MHz, and for different values of σ. **a** A strongly localised modulation ($\sigma = 0.02$) leads to the formation of a narrow bandwidth OFC spectrum with a few comb resonances. **b**, **c** The bandwidth of the frequency comb spectrum increases with the width σ of the SDPMs. **d** The optimal spectrum with largest bandwidth is achieved at $\sigma \sim 0.3$. **e** The bandwidth of the OFC starts to decrease when the value of σ is further increased. This case corresponds to a parabolic SDPM since $\xi(z/L) = e^{-(z/\sigma L)^2} \approx (z/L)^2$ for $\sigma = 1$. **f** The generation of combs is strongly suppressed in the case of a uniform SDPM.

to $\nu_{\mathrm{in}} = \nu_{q_0} = 200$ THz, where the axial mode number is $q_0 = 50$. From the scaling relation $\Delta r_0 = r_0\Delta\nu_0/\nu_{q_0}$, the ERV of the SBM considered is $\Delta r_0 = 2$ nm, as in the adiabatic case. The attenuation factor and coupling coefficient are set to $\gamma = 2\pi$ MHz and $D_0 = 0.001(1+\mathrm{i})\ \mu\mathrm{m}^{-1}$. The corresponding Q-factor of mode q_0 calculated from Eqs. (5) and (6) is $Q_{q_0} = 3\times 10^7$.

The results of our numerical modelling of Eq. (3) are shown in Fig. 5. As in the adiabatic case, the OFCs are generated by the Gaussian SDPM determined by $\xi(z/L) = e^{-(z/\sigma L)^2}$ with dimensionless widths σ varying from 0.02 to 10. We consider two modulation amplitude maxima, $\delta\nu_{\mathrm{par}} = 0.04\Delta\nu_0 = 200$ MHz and $\delta\nu_{\mathrm{par}} = 0.015\Delta\nu_0 = 75$ MHz, which are much smaller than the maximum CFV of the SBM $\Delta\nu_0$. From the scaling relation $\delta r_{\mathrm{par}} = r_0\delta\nu_{\mathrm{par}}/\nu_{c0}$, these amplitudes correspond to the ERV $\delta r_{\mathrm{par}} = 80$ pm and $\delta r_{\mathrm{par}} = 30$ pm, respectively. Contrary to the

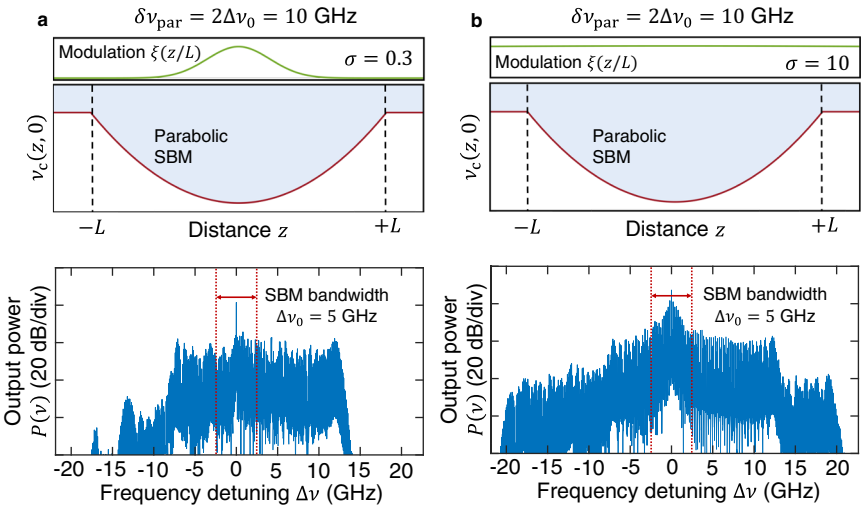

Fig. 6 Optical frequency combs (OFCs) generated by parametric modulations with Gaussian spatial distributions and amplitude exciding the bandwidth of the SNAP bottle microresonator (SBM). a The parabolic SNAP bottle microresonator (SBM) (red line) is parametrically modulated with a Gaussian modulation profile $\xi(z/L) = e^{-(z/\sigma L)^2}$ (green line) with $\sigma = 0.3$. The amplitude of the modulation exceeds the bandwidth of the SBM, $\delta\nu_{\rm par} = 2\Delta\nu_0 = 10$ GHz. The OFC spectrum generated is several times larger than the SBM bandwidth $\Delta\nu_0 = 5$ GHz. **b** A close to uniform modulation ($\sigma = 10$) is used to parametrically modulate the parabolic SBM. The bandwidth of the resulting OFC spectrum is several times wider than the SBM bandwidth. Unlike the case of small modulation amplitudes, the frequency comb spectrum generated is comparable to the case $\sigma = 0.3$.

adiabatic case, the OFC spectral bandwidth behaves nonmonotonically as a function of σ. It is seen from Fig. 5 that, with increasing the SDPM width from very narrow at $\sigma = 0.02$ (Fig. 5a), the OFC spectral bandwidth first becomes wider (Fig. 5b, c), reaches the optimum profile at around $\sigma = 0.3$ (Fig. 5d), and then shrinks down (Fig. 5e) and vanishes for the practically uniform SDPM at $\sigma = 10$ (Fig. 5f). Vanishing of the OFC spectral bandwidth for narrow SDPM (Fig. 5a) is straightforwardly explained by the reduction of integrated modulation power. The less obvious suppression of the OFC generation for the SDPM approaching the uniform distribution (Fig. 5f) can be clarified with the help of the quantum and semiclassical perturbation theory. Indeed, the transition between SBM axial modes with different quantum numbers q caused by the spatially uniform perturbation is strongly suppressed due to the orthogonality of these modes. For example, in the first order of the quantum perturbation theory, the transition from mode $\varphi_{q_1}(z)\exp(i\nu_{q_1}t)$ to mode $\varphi_{q_2}(z)\exp(i\nu_{q_2}t)$ under the perturbation $W(z)\sin(2\pi\nu_{\rm par}t)$ (see Eq. (2)) is proportional to $\langle\varphi_{q_1}|W|\varphi_{q_2}\rangle$[36]. For the constant perturbation, $W(z) = W_0$, we have $\langle\varphi_{q_1}|W|\varphi_{q_2}\rangle = W_0\langle\varphi_{q_1}|\varphi_{q_2}\rangle = 0$ due to the orthogonality of φ_{q_1} and φ_{q_2}.

Similar to the previous section, in addition to the cases of relatively small modulation amplitudes $\delta\nu_{\rm par} \ll \Delta\nu_0$, it is interesting to investigate the case when $\delta\nu_{\rm par}$ is comparable to the full CFV $\Delta\nu_0$. As an example, Fig. 6 compares the OFC spectra generated by the same SBM modulated with maximum amplitude $\delta\nu_{\rm par} = 2\Delta\nu_0 = 10$ GHz and Gaussian profile $\xi(z/L) = e^{-(z/\sigma\cdot L)^2}$. Figure 6a shows the case with $\sigma = 0.3$ (optimal for the relatively weak modulation, see Fig. 5d) and Fig. 6b shows the case of close to uniform SDPM with $\sigma = 10$. It is seen that, contrary to the case of relatively small modulation amplitude, the uniform modulation generates an OFC which is, in general, comparable with that for $\sigma = 0.3$. However, the OFC spectrum for $\sigma = 0.3$ is closer to uniform and on average has a greater power over the larger bandwidth. We suggest that an OFC profile with better flatness and larger bandwidth can be achieved with an optimization using a more complex SDPM. The detailed solution of this problem and the investigation of effects induced by larger vibrations of SBMs, such as change of their temperature and other physical characteristics[37], is beyond the scope of this paper.

Conclusion

Parametric modulation of optical microresonators is a promising approach for the generation of optical frequency combs (OFCs) which has been demonstrated in spherical[15], ring (racetrack)[19,20], and toroidal[15,18] microresonators. The repetition rate of the OFC excited by these resonators is inverse proportional to their perimeter so that the OFCs with the characteristic repetition rate smaller than a gigahertz correspond to resonators with macroscopically large dimensions (see Introduction for details). However, it was proposed in refs. [33,34,38] that a SNAP bottle microresonator (SBM) with much smaller dimensions can be used to generate OFCs with repetition rate below a gigahertz.

In this paper, we consider the generation of OFCs in a parabolic SBM by the modulation of its parameters. The main difference of an SBM compared to spherical and toroidal microresonators consists in its strong axial elongation. For this reason, the spatial distribution of the parametric modulation (SDPM) along the SBM axis becomes of major importance. Furthermore, the characteristic parametric modulation of the effective radius variation (ERV), $\delta r_{\rm par}$, can be comparable or larger than the dramatically small nanometre-scale ERV Δr_0 of the SBMs considered. In our numerical simulations, we investigate the effect of the SDPM assuming that it has a Gaussian shape. In the adiabatic case, when the modulation frequency is much smaller than the axial free spectral range (FSR), $\nu_{\rm par} \ll \Delta\nu_{\rm FSR}$, we show that a uniform SDPM produces the OFC with the best flatness and largest spectral bandwidth (Fig. 3f). An adiabatic SDPM with uniform amplitude $\delta r_{\rm par} \geq \Delta r_0$ generates a relatively flat OFC with bandwidth proportional to this amplitude (Fig. 4). For resonant modulation, $\nu_{\rm par} = 2\Delta\nu_{\rm FSR}$, with a relatively small amplitude, $\delta r_{\rm par} \ll \Delta r_0$, the OFC disappears both for very narrow and uniform SDPM as shown in Fig. 5a, f. However, the OFC can achieve an optimal shape with the best flatness and largest bandwidth at an intermediate SDPM width, as depicted in Fig. 5d. Our study only includes symmetric SDPMs. However, the behaviour of asymmetric SDPMs may differ significantly, particularly in the resonant case, as

the spatial coupling of modes would be altered. For instance, a spatially antisymmetric modulation could couple modes with different symmetry. More complex SDPM profiles may, therefore, lead to changes in the process of OFC generation that are non-intuitive and difficult to predict. For larger modulation amplitudes, $\delta r_{par} \geq \triangle r_0$, the resonant modulation with a nonuniform SDPM results in a flater OFC with a broader bandwidth compared to that generated by the uniform SDPM (Fig. 6). We suggest that an SDPM with a more complex dependence on the axial coordinate, which takes into account the actual axial distribution of the SBM modes, may lead to a better OFC optimization.

The optimized generation of OFCs by an SBM proposed in this paper can be realized experimentally by one of the following approaches. First, modulation of the refractive index and radiation pressure of an SBM can be induced by the input resonant pump light harmonically modulated with frequency ν_{par}. To ensure the resonant enhancement of the pump light, its spectrum should be localized near an SBM cutoff frequency ν_{cp}. While the case when the pump light induces the OFC directly (i.e., when $\nu_{cp} = \nu_{c0}$, see Eq. (2)) is of special interest, we assumed in this paper that the cutoff frequencies ν_{cp} and ν_{c0} (as well as the spectrum of the pump light and the frequency ν_{in} of a relatively weak input light) are separated so that the spectrum of pump light and the spectrum of the generated OFC do not overlap. The required spatial distribution of the pump light can be achieved by adjusting its spectrum. Second, the adiabatic excitation of the OFCs can be performed in a way similar to that demonstrated by Hu et al.[22] by excitation of acoustic modes of an SBM with a strong pump light. Third, assuming that the ultraprecise fabrication of an SBM of material with strong second-order nonlinearities may become possible, the refractive index modulation can be performed by applying a periodic electric field to the SBM fabricated of such material[18]. Finally, an SBM can be fabricated at the surface of a microcapillary filled with such highly nonlinear or piezoelectric material, which can be used to mechanically modulate the SBM parameters[39].

Overall, complementary to the spherical, ring, and toroidal microresonators, the elongated SBMs allows us to change the SDPM and optimise the OFC spectrum. In the case of adiabatic parametric modulation, it is possible to tune the repetition rate of the OFC without changing the SBM profile by modifying the modulation frequency ν_{par}. In the case of the resonant parametric modulation, the repetition rate frequency is determined and fixed by the FSR of the SBM, which can be made much smaller that the FSR of other microresonators with similar dimensions. In both cases, for relatively weak modulation amplitude, the comb bandwidth is limited by the bandwidth of discrete eigenfrequencies of the SBM considered.

Methods

Generation of OFCs by a spatially uniform parametric modulation. We consider a cutoff frequency that depends on time and position as $\nu_c(z,t) = \nu_{c0} + \Delta\nu(z) + \delta\nu_{\mathrm{par}} \cdot \sin(2\pi\nu_{\mathrm{par}}t)$, where $|\Delta\nu(z)| \ll \nu_{c0}$ and $\delta\nu_{\mathrm{par}} = const$. After the substitution

$$\Psi(z,t) = \psi(z,t)\mathrm{e}^{\frac{\mathrm{i}\delta\nu_{\mathrm{par}}}{\nu_{\mathrm{par}}}\cos\left(2\pi\nu_{\mathrm{par}}t\right)}, \tag{9}$$

Equation (3) can be written as

$$\left[\mathrm{i}\frac{1}{2\pi}\partial_t - \hat{L}\right]\psi(z,t) = S(z,t) \tag{10a}$$

$$\hat{L} = -\frac{1}{2}\kappa\partial_z^2 + \left(\nu_{c0} - \nu_{\mathrm{in}} + \Delta\nu(z) - \mathrm{i}\gamma\right) - \kappa D_0\delta(z - z_0) \tag{10b}$$

$$S(z,t) = \nu_{c0}A_{\mathrm{in}}(z,t)\mathrm{e}^{-\frac{\mathrm{i}\delta\nu_{\mathrm{par}}}{\nu_{\mathrm{par}}}\cos\left(2\pi\nu_{\mathrm{par}}t\right)} \tag{10c}$$

where $\kappa = \nu_{c0}/\beta_{c0}^2$. For the parabolic CFV, $\Delta\nu(z) = \Delta\nu_0[(\frac{z}{L})^2 - 1]$, we search for solution of Eq. (10a) in the form

$$\psi(z,t;z_0) = \sum_q \varphi_q(z)\varphi_q^*(z_0)a_q(t) \tag{11}$$

where $a_q(t)$ are functions of time to be determined and $\varphi_q(z)$ are the normalised eigenfunctions of the operator $\hat{L}$ with associated eigenfrequencies ς_q. For finite material loss γ and coupling D_0 considered, the eigenfrequencies are complex-valued and equal to $\varsigma_q = \nu_q - \nu_{\mathrm{in}} - \mathrm{i}\Gamma_q$ (see Eqs. (4) and (5)). Nevertheless, due to the relatively small values of γ and $\mathrm{Im}(D_0)$ assumed, the normalization of $\varphi_q(z)$ and their orthogonality can be achieved with the required accuracy.

In order to determine $a_q(t)$, we substitute Eq. (11) into Eq. (10a),

$$\sum_q \varphi_q(z)\varphi_q^*(z_0)\left[\mathrm{i}\frac{1}{2\pi}\frac{\mathrm{d}}{\mathrm{d}t}a_q(t) - \varsigma_q a_q(t)\right] = S(z,t), \tag{12}$$

multiply each side of Eq. (12) by $\varphi_q^*(z)$ and integrate over z. As a result, we arrive at the following equations for $a_q(t)$:

$$\frac{1}{2\pi}\frac{\mathrm{d}}{\mathrm{d}t}a_q(t) + \mathrm{i}\varsigma_q a_q(t) = -\mathrm{i}\nu_{c0}A_0\left(1 - \mathrm{e}^{-\alpha t}\right)\mathrm{e}^{-\mathrm{i}\frac{\delta\nu_{\mathrm{par}}}{\nu_{\mathrm{par}}}\cos\left(2\pi\nu_{\mathrm{par}}t\right)} \tag{13}$$

with initial conditions $a_q(t=0) = A_{\mathrm{in}}(z,0) = 0$. Solving these equations and application of the Jacobi-Anger expansion[40], results in the following solution of Eq. (3) at $z = z_0$:

$$\Psi(z_0,t) = \nu_{c0}A_0\sum_q\left|\varphi_q(z_0)\right|^2\sum_n\sum_m(-1)^m\mathrm{i}^n J_{n-m}\left(\frac{\delta\nu_{\mathrm{par}}}{\nu_{\mathrm{par}}}\right) J_m\left(\frac{\delta\nu_{\mathrm{par}}}{\nu_{\mathrm{par}}}\right)\frac{e^{2\pi\mathrm{i}n\nu_{\mathrm{par}}t}}{\left(\nu_q - \nu_{\mathrm{in}} + m\nu_{\mathrm{par}}\right) - \mathrm{i}\Gamma_q}. \tag{14}$$

We assume now that the input frequency ν_{in} is situated in a small vicinity of one of the SBM frequencies ν_{q_0} of the order of the resonance width, $|\nu_{\mathrm{in}} - \nu_{q_0}| \sim \Gamma_{q_0}$, and the excited OFC resonances are well defined so that $\Gamma_{q_0} \ll \nu_{\mathrm{par}}$. In addition, we assume that none of the SBM frequencies ν_q, except for ν_{q_0}, are close to the parametrically modulated OFC resonances. Such situation may occur for adiabatic modulation, when $\nu_{\mathrm{par}} \ll \Delta\nu_{\mathrm{FSR}}$. Then, Eq. (14) is reduced to

$$\Psi(z_0,t) = \sum_n \Psi_n e^{2\pi\mathrm{i}n\nu_{\mathrm{par}}t}, \tag{15}$$

where

$$\Psi_n = \mathrm{i}^{n+1}\frac{\nu_{c0}}{\Gamma_{q_0}}A_0\left|\varphi_{q_0}(z_0)\right|^2 J_n\left(\frac{\delta\nu_{\mathrm{par}}}{\nu_{\mathrm{par}}}\right)J_0\left(\frac{\delta\nu_{\mathrm{par}}}{\nu_{\mathrm{par}}}\right). \tag{16}$$

In particular, at zero modulation, we have:

$$\Psi(z_0,t) = \Psi_0 = \mathrm{i}\frac{\nu_{c0}}{\Gamma_{q_0}}A_0\left|\varphi_{q_0}(z_0)\right|^2. \tag{17}$$

Substitution of Eqs. (16), (17) into Eq. (7) yields Eq. (8).

Numerical solution of the Schrödinger equation. The Schrödinger equation is solved using the Fourier split-step method[41], which can be briefly described as follows. We first rewrite Eq. (3) as ref. [42]:

$$\mathrm{i}\partial_\tau\hat{\Psi} = -\frac{1}{2}\partial_x^2\hat{\Psi} + \frac{1}{2}V_0\left[x^2 + \delta\hat{\nu}_{\mathrm{par}}x_c^2\xi(x/x_c)\right]\hat{\Psi} + \Delta\hat{\nu}\hat{\Psi} - \mathrm{i}\hat{\gamma}\hat{\Psi} - \hat{D}_0\delta(x - x_0)\hat{\Psi} + \hat{A}_{\mathrm{in}}(x,\tau) \tag{18}$$

In this equation, we have introduced the dimensionless variables $\tau = t/T_0$, $x = z/L_0$ and $\hat{\Psi} = \Psi/I_0$, where T_0, L_0 and I_0 are the scaling factors. The dimensionless parameters in Eq. (18) are defined as $V_0 = 8\pi^2\Delta\nu_0\nu_{c0}n_0^2L_0^4/c^2L^2$, $\delta\hat{\nu}_{\mathrm{par}} = \delta\nu_{\mathrm{par}}/\Delta\nu_0$, $x_c = L/L_0$, $\Delta\hat{\nu} = 2\pi(\Delta\nu_0 + \nu_{c0} - \nu_{\mathrm{par}})T_0$, $\hat{\gamma} = 2\pi\gamma T_0$, $\hat{D}_0 = L_0D_0$ and $\hat{A}_{\mathrm{in}}(x,\tau) = 2\pi\nu_{c0}T_0/L_0I_0 \cdot A_{\mathrm{in}}(x,\tau)$.

We can split the r.h.s. of Eq. (18) into the momentum space component

$$\hat{\mathrm{D}} = -\frac{1}{2}\partial_x^2 \tag{19}$$

and the position space component

$$\hat{\mathrm{N}} = \frac{1}{2}V_0\left[x^2 + \delta\hat{\nu}_{\mathrm{par}}x_c^2\xi(x/x_c)\right] + \Delta\hat{\nu} - \mathrm{i}\hat{\gamma} - \hat{D}_0\delta(x - x_0) \tag{20}$$

and rewrite Eq. (18) in terms of these two operators as:

$$\mathrm{i}\partial_\tau\hat{\Psi} = \left[\hat{\mathrm{D}} + \hat{\mathrm{N}}\right]\hat{\Psi} + \hat{A}_{\mathrm{in}}(x,\tau) \tag{21}$$

For a small time step $\Delta\tau$, the solution of this equation can be approximated as

$$\hat{\Psi}(\tau + \Delta\tau) = \mathrm{e}^{-\mathrm{i}\Delta\tau\hat{\mathrm{D}}}\mathrm{e}^{-\mathrm{i}\Delta\tau\hat{\mathrm{N}}}\hat{\Psi}(\tau) - \mathrm{i}\Delta\tau\hat{A}_{\mathrm{in}}(x,\tau) \tag{22}$$

with an error of the order of $\Delta\tau^2$. To compute the term associated to the operator

$\hat{D}$, we use the spatial fast Fourier transform (FFT) of the field $\hat{\Psi}$:

$$\hat{D}\hat{\Psi} = \mathrm{FFT}^{-1}\left\{e^{-\frac{ik^2}{2}}\mathrm{FFT}\left(\hat{\Psi}\right)\right\} \quad (23)$$

where k represents the coordinate in the reciprocal space. We solve Eq. (22) with a uniform space grid of $N = 2^n$ points defined as $x_n = n\Delta x$, with $n \in [-N/2, N/2-1]$. The points in the reciprocal space are defined as $k_n = 2\pi n/\Delta x N$.

Data availability

The data that support the plots of this paper and other findings within this study are available from the corresponding author upon reasonable request.

Code availability

No original algorithms or codes have been developed for this article. The MATLAB program used for processing the data is nevertheless available from the corresponding author on reasonable request.

Received: 31 October 2022; Accepted: 3 March 2023;
Published online: 21 March 2023

References

1. Fortier, T. & Baumann, E. 20 years of developments in optical frequency comb technology and applications. *Commun. Phys.* **2**, 1–16 (2019).
2. Diddams, S. A., Vahala, K. & Udem, T. Optical frequency combs: coherently uniting the electromagnetic spectrum. *Science* **369**, eaay3676 (2020).
3. Picqué, N. & Hänsch, T. W. Frequency comb spectroscopy. *Nat. Photon.* **13**, 146–157 (2019).
4. Wilson, N. et al. Simultaneous observation of bonlinear magneto-optical rotation in the temporal and spectral domains with an electro-optic frequency comb. *Phys. Rev. Appl.* **10**, 034012 (2018).
5. Udem, T., Holzwarth, R. & Hänsch, T. W. Optical frequency metrology. *Nature* **416**, 233–237 (2002).
6. Marin-Palomo, P. et al. Microresonator-based solitons for massively parallel coherent optical communications. *Nature* **546**, 274–279 (2017).
7. Droste, S., Ycas, G., Washburn, B. R., Coddington, I. & Newbury, N. R. Optical frequency comb generation based on Erbium fiber lasers. *Nanophotonics* **5**, 196–213 (2016).
8. Carlson, D. R. et al. Ultrafast electro-optic light with subcycle control. *Science* **361**, 1358–1363 (2018).
9. Pasquazi, A. et al. Micro-combs: a novel generation of optical sources. *Phys. Rep.* **729**, 1–81 (2018).
10. Gaeta, A. L., Lipson, M. & Kippenberg, T. J. Photonic-chip-based frequency combs. *Nat. Photon.* **13**, 158–169 (2019).
11. Kippenberg, T. J., Gaeta, A. L., Lipson, M. & Gorodetsky, M. L. Dissipative Kerr solitons in optical microresonators. *Science* **361**, eaan8083 (2018).
12. Del'Haye, P. et al. Optical frequency comb generation from a monolithic microresonator. *Nature* **450**, 1214–1217 (2007).
13. Herr, T. et al. Temporal solitons in optical microresonators. *Nat. Photonics* **8**, 145–152 (2014).
14. Herr, T. et al. Universal formation dynamics and noise of Kerr-frequency combs in microresonators. *Nat. Photon.* **6**, 480–487 (2012).
15. Ilchenko, V. S., Savchenkov, A. A., Matsko, A. B. & Maleki, L. Whispering-gallery-mode electro-optic modulator and photonic microwave receiver. *J. Opt. Soc. Am. B* **20**, 333 (2003).
16. Rokhsari, H., Kippenberg, T. J., Carmon, T. & Vahala, K. J. Radiation-pressure-driven micro-mechanical oscillator. *Opt. Express* **13**, 5293–5301 (2005).
17. Carmon, T., Rokhsari, H., Yang, L., Kippenberg, T. J. & Vahala, K. J. Temporal behavior of radiation-pressure-induced vibrations of an optical microcavity phonon mode. *Phys. Rev. Lett.* **94**, 223902 (2005).
18. Rueda, A., Sedlmeir, F., Kumari, M., Leuchs, G. & Schwefel, H. G. L. Resonant electro-optic frequency comb. *Nature* **568**, 378–381 (2019).
19. Zhang, M. et al. Broadband electro-optic frequency comb generation in a lithium niobate microring resonator. *Nature* **568**, 373–377 (2019).
20. Buscaino, B., Zhang, M., Lončar, M. & Kahn, J. M. Design of efficient resonator-enhanced electro-optic frequency vcomb generators. *J. Light. Technol.* **38**, 1400–1413 (2020).
21. Bao, Y. et al. A digitally generated ultrafine optical frequency comb for spectral measurements with 0.01-pm resolution and 0.7-μs response time. *Light Sci. Appl.* **4**, e300–e300 (2015).
22. Hu, Y. et al. Generation of optical frequency comb via giant optomechanical oscillation. *Phys. Rev. Lett.* **127**, 134301 (2021).
23. Sumetsky, M. Theory of SNAP devices: basic equations and comparison with the experiment. *Opt. Express* **20**, 22537–22554 (2012).
24. Sumetsky, M. Optical bottle microresonators. *Prog. Quantum Electron.* **64**, 1–30 (2019).
25. Gardosi, G., Mangan, B. J., Puc, G. S. & Sumetsky, M. Photonic microresonators created by slow optical cooking. *ACS Photonics* **8**, 436–442 (2021).
26. Yu, Q. et al. Rectangular SNAP microresonator fabricated with a femtosecond laser. *Opt. Lett.* **44**, 5606–5609 (2019).
27. Toropov, N., Zaki, S., Vartanyan, T. & Sumetsky, M. Microresonator devices lithographically introduced at the optical fiber surface. *Opt. Lett.* **46**, 1784–1787 (2021).
28. Sumetsky, M. Delay of light in an optical bottle resonator with nanoscale radius variation: dispersionless, broadband, and low loss. *Phys. Rev. Lett.* **111**, 163901 (2013).
29. Yin, Y., Niu, Y., Qin, H. & Ding, M. Kerr frequency comb generation in microbottle resonator with tunable zero dispersion wavelength. *J. Light. Technol.* **37**, 5571–5575 (2019).
30. Jin, X. et al. Controllable two-dimensional Kerr and Raman-Kerr frequency combs in microbottle resonators with selectable dispersion. *Photon. Res.* **9**, 171–180 (2021).
31. Wang, M. et al. Experimental demonstration of nonlinear scattering processes in a microbottle resonator based on a robust packaged platform. *J. Light. Technol.* **39**, 5917–5924 (2021).
32. Savchenkov, A. A. et al. Kerr combs with selectable central frequency. *Nat. Photon.***5**, 293–296 (2011).
33. Suchkov, S. V., Sumetsky, M. & Sukhorukov, A. A. Frequency comb generation in SNAP bottle resonators. *Opt. Lett.* **42**, 2149–2152 (2017).
34. Sumetsky, M. Optical frequency combs generated mechanically. *Opt. Lett.* **42**, 3197–3200 (2017).
35. Sumetsky, M. Microscopic optical buffering in a harmonic potential. *Sci. Rep.* **5**, 18569 (2015).
36. Landau, L. D. & Lifshitz, E. M. *Quantum Mechanics: Non-Relativistic Theory* (Elsevier, 1981).
37. Fultz, B. Vibrational thermodynamics of materials. *Prog. Mater. Sci.* **55**, 247–352 (2010).
38. Dvoyrin, V. & Sumetsky, M. Bottle microresonator broadband and low-repetition-rate frequency comb generator. *Opt. Lett.* **41**, 5547–5550 (2016).
39. Dmitriev, A. V. & Sumetsky, M. Tunable photonic elements at the surface of an optical fiber with piezoelectric core. *Opt. Lett.* **41**, 2165–2168 (2016).
40. Abramowitz, M. & Stegun, I. A. *Handbook of Mathematical Functions: With Formulas, Graphs, and Mathematical Tables* (Courier Corporation, 1965).
41. Agrawal, G. P. *Nonlinear Fiber Optics* (Academic Press, 2012).
42. Crespo-Ballesteros, M. & Sumetsky, M. Controlled transportation of light by light at the microscale. *Phys. Rev. Lett.* **126**, 153901 (2021)..

Acknowledgements

The work of M.C.-B. and M.S. was supported by the Engineering and Physical Sciences Research Council (EPSRC) (grants EP/P006183/1 and EP/W002868/1) and Leverhulme Trust (grant RPG-2022-014). The reported research performed by A.B.M. was carried out at the Jet Propulsion Laboratory, California Institute of Technology, under a contract with the National Aeronautics and Space Administration (80NM0018D0004).

Author contributions

M.C.-B. and M.S. developed the original theoretical model which was further justified in discussions with A.B.M. The numeral simulations were conducted by M.C.-B. All authors participated in discussions of the numerical results. The original draft of the paper was prepared by M.C.-B. which was reviewed and edited by M.S. and A.B.M. The idea of the project was conceived by M.S.

Competing interests

The authors declare no competing interests.

Additional information

Correspondence and requests for materials should be addressed to Manuel Crespo-Ballesteros.

Peer review information *Communications Physics* thanks the anonymous reviewers for their contribution to the peer review of this work.

Reprints and permission information is available at http://www.nature.com/reprints

Publisher's note Springer Nature remains neutral with regard to jurisdictional claims in published maps and institutional affiliations.